Supplementary Materials - A Decoupled Model Predictive Control for Path Following on Complex Surfaces

João Cavalcanti Santos, Lénaïc Cuau, Philippe Poignet, Nabil Zemiti

Supplementary Materials
A Decoupled Model Predictive Control for Path Following on Complex Surfaces

João Cavalcanti Santos, Lenaïc Cuau, Philippe Poignet, Nabil Zemiti

January 30, 2023

This article presents supplementary materials of the paper entitled *A Decoupled Model Predictive Control for Path Following on Complex Surfaces*, published in IEEE Robotics and Automation Letters, 2023. Sections, equations, figures and references are numbered such as the numbering is consistent with the main paper.

A proof of convergence of Algorithm 1 is performed in Section A. The capability of the proposed control scheme to track self-intersecting curves is discussed in Section B. Finally, Section C presents further details on the integration of external controllers to the proposed PPFC.

Contents

A Convergence of Algorithm 1

The convergence of Algorithm 1 can be proved based on the assumption that each of the steps $\|\mathbf{p}_{d,k+1} - \mathbf{p}_{d,k}\|$ are finite, which is the typical application of the proposed control scheme. A detailed discussion on this matter is presented in the following.

Theorem 1: *Consider any given sequence of desired points* $\mathcal{P}_d = \{\mathbf{p}_{d,1},\, \mathbf{p}_{d,2}, \dots\}$, *end-effector position* $\mathbf{p} \in \mathbb{R}^3$ *and positive integer* k_0. *If there is a positive scalar* ε *such that*

$$\Delta p_{d,k} = \|\mathbf{p}_{d,k+1} - \mathbf{p}_{d,k}\| \geqslant \varepsilon > 0, \forall\, k \in \{k_0,\, k_0 + 1, \dots\} \tag{23}$$

then the Algorithm 1 converges to a positive integer $\hat{k} \geqslant k_0$.

Proof of Theorem 1. Consider a given $k \geqslant k_0$ such that

$$\mathbf{e}_j^T\,(\mathbf{p} - \mathbf{p}_{d,j}) \geqslant \Delta p_{d,j}\, \forall\, j \in \{k_0, k_0 + 1, \dots, k\}. \tag{24}$$

with $\mathbf{e}_j = (\mathbf{p}_{d,j+1} - \mathbf{p}_{d,j})/\|\mathbf{p}_{d,j+1} - \mathbf{p}_{d,j}\|$. This represents a case in which a `true` value for the condition

$$\lambda_j = \mathbf{e}_j^T(\mathbf{p} - \mathbf{p}_{d,j}) \geqslant \Delta p_{d,j} \tag{25}$$

was obtained in step 3 of Algorithm 1 for $j \in \{k_0, k_0 + 1, \dots, k\}$. The solution of Algorithm 1 is obtained when $j = \hat{k}$ such that (25) is violated (`false` value in step 3).

Let $\mathcal{V}_{k+1}$ be the defined as

$$\mathcal{V}_{k+1} = \Bigg\{ \mathbf{v} \in \mathbb{R}^3 \,:$$

$$\|\mathbf{v} - \mathbf{p}_{d,k}\| \geqslant \varepsilon \text{ and} \tag{26a}$$

$$\left(\frac{\mathbf{v} - \mathbf{p}_{d,k}}{\|\mathbf{v} - \mathbf{p}_{d,k}\|}\right)^T (\mathbf{p} - \mathbf{p}_{d,k}) \geqslant \|\mathbf{v} - \mathbf{p}_{d,k}\| \Bigg\}. \tag{26b}$$

The set $\mathcal{V}_{k+1}$ is used to study the conditions on which $\mathbf{v} = \mathbf{p}_{k+1}$ will lead to a `false` or `true` value in condition (25) for $j = k + 1$. Thanks to (26b),

$$\mathbf{p}_{d,k+1} \in \mathcal{V}_{k+1} \Leftrightarrow$$
$$\left(\frac{\mathbf{p}_{d,k+1} - \mathbf{p}_{d,k}}{\|\mathbf{p}_{d,k+1} - \mathbf{p}_{d,k}\|}\right)^T (\mathbf{p} - \mathbf{p}_{d,k}) = \mathbf{e}_k^T(\mathbf{p} - \mathbf{p}_{d,k}) \geqslant \|\mathbf{p}_{d,k+1} - \mathbf{p}_{d,k}\| = \Delta p_{d,k},$$

leading to a `true` value of condition (25). Conversely, since (23) implies that $\mathbf{v} = \mathbf{p}_{d,k+1}$ necessarily satisfies (26a), then

$$\mathbf{p}_{d,k+1} \notin \mathcal{V}_{k+1} \Leftrightarrow \mathbf{e}_k^T(\mathbf{p} - \mathbf{p}_{d,k}) < \|\mathbf{p}_{d,k+1} - \mathbf{p}_{d,k}\| = \Delta p_{d,k},$$

which implies that a `false` value is obtained in step 3 of Algorithm 1 for k, thus converging to $\hat{k} = k$. Note also that the combination of (26a) and (26b) leads to

$$d_k = \|\mathbf{p} - \mathbf{p}_{d,k}\| < \varepsilon \Rightarrow \mathcal{V}_{k+1} = \{\varnothing\} \Rightarrow \mathbf{p}_{d,k+1} \notin \mathcal{V}_{k+1}. \tag{27}$$

In short, (27) implies that $d_k < \varepsilon$ leads to a `false` value in condition (25).

The Theorem 1 is proved showing that $\mathcal{V}_k$ shrinks of a finite volume for each step of Algorithm 1. This is proved studying the upper bounds of the sequence

$$d_k = \|\mathbf{p} - \mathbf{p}_{d,k}\|. \tag{28}$$

To do so, consider the maximum value $\overline{d}_{k+1}$ that the expression $d_{k+1} = \|\mathbf{p} - \mathbf{p}_{d,k+1}\|$ can lead for any $\mathbf{p}_{d,k+1} \in \mathcal{V}_{k+1}$ for given $\mathbf{p}$ and $\mathbf{p}_{d,k}$. The value of $\overline{d}_{k+1}$ can be computed according to

$$\overline{d}_{k+1} = \max_{\mathbf{v}\in\mathbb{R}^3} \|\mathbf{v} - \mathbf{p}\| \tag{29a}$$

$$\text{s.t. } \|\mathbf{v} - \mathbf{p}_{d,k}\| \geqslant \varepsilon \text{ and} \tag{29b}$$

$$\left(\frac{\mathbf{v} - \mathbf{p}_{d,k}}{\|\mathbf{v} - \mathbf{p}_{d,k}\|}\right)^T (\mathbf{p} - \mathbf{p}_{d,k}) \geqslant \|\mathbf{v} - \mathbf{p}_{d,k}\|. \tag{29c}$$

After some straightforward manipulations, the first order Karush–Kuhn–Tucker optimality conditions [30, Section 12.3] for the problem (29) can be written as

$$(\mathbf{v} - \mathbf{p}) + \lambda_1 (\mathbf{v} - \mathbf{p}_{d,k}) + \lambda_2 \Big((\mathbf{p} - \mathbf{p}_{d,k}) - 2(\mathbf{v} - \mathbf{p}_{d,k})\Big) = \mathbf{0} \tag{30a}$$

$$f_1(\mathbf{v}) = \|\mathbf{v} - \mathbf{p}_{d,k}\| - \varepsilon \geqslant 0 \tag{30b}$$

$$f_2(\mathbf{v}) = \frac{(\mathbf{v} - \mathbf{p}_{d,k})^T}{\|\mathbf{v} - \mathbf{p}_{d,k}\|} (\mathbf{p} - \mathbf{p}_{d,k}) - \|\mathbf{v} - \mathbf{p}_{d,k}\| \geqslant 0 \tag{30c}$$

$$\lambda_1 \geqslant 0 \tag{30d}$$

$$\lambda_2 \geqslant 0 \tag{30e}$$

$$\lambda_1 f_1(\mathbf{v}) = 0 \tag{30f}$$

$$\lambda_2 f_2(\mathbf{v}) = 0 \tag{30g}$$

The solutions of (30) can be summarized into the following three sets:

$$\text{(I)} \Rightarrow \begin{cases} \mathbf{v} \in \mathbb{R}^3 : \begin{cases} (\mathbf{v} - \mathbf{p}_{d,k})^T (\mathbf{v} - \mathbf{p}_{d,k}) = \varepsilon^2 \\ (\mathbf{v} - \mathbf{p}_{d,k})^T (\mathbf{p} - \mathbf{p}_{d,k}) = \varepsilon^2 \end{cases} \\ \lambda_1 = \lambda_2 = 1 \end{cases} \tag{31}$$

$$\text{(II)} \Rightarrow \begin{cases} \mathbf{v} = \mathbf{p}_{d,k} + \frac{\mathbf{p} - \mathbf{p}_{d,k}}{\|\mathbf{p} - \mathbf{p}_{d,k}\|} \varepsilon \\ \lambda_1 = 1 - \frac{\mathbf{p} - \mathbf{p}_{d,k}}{\varepsilon} \\ \lambda_2 = 0 \end{cases} \tag{32}$$

$$\text{(III)} \Rightarrow \begin{cases} \mathbf{v} = \mathbf{p} \\ \lambda_1 = \lambda_2 = 0 \end{cases} \tag{33}$$

The square of the cost function (29a) for a solution $\mathbf{v} = \mathbf{v}_{(\mathrm{I})}$ of case (I) can be rewritten as

$$\begin{gathered}\|\mathbf{v}_{(\mathrm{I})} - \mathbf{p}\|^2 = (\mathbf{v}_{(\mathrm{I})} - \mathbf{p})^T(\mathbf{v}_{(\mathrm{I})} - \mathbf{p}) = \\ (\mathbf{v}_{(\mathrm{I})} - \mathbf{p}_{d,k} + \mathbf{p}_{d,k} - \mathbf{p})^T(\mathbf{v}_{(\mathrm{I})} - \mathbf{p}_{d,k} + \mathbf{p}_{d,k} - \mathbf{p}) = \\ \underbrace{(\mathbf{v}_{(\mathrm{I})} - \mathbf{p}_{d,k})^T(\mathbf{v}_{(\mathrm{I})} - \mathbf{p}_{d,k})}_{\varepsilon^2} - 2\underbrace{(\mathbf{v}_{(\mathrm{I})} - \mathbf{p}_{d,k})^T(\mathbf{p} - \mathbf{p}_{d,k})}_{\varepsilon^2} + \underbrace{(\mathbf{p} - \mathbf{p}_{d,k})^T(\mathbf{p} - \mathbf{p}_{d,k})}_{d_k^2} = \\ \varepsilon^2 - 2\,\varepsilon^2 + d_k^2 = \\ d_k^2 - \varepsilon^2\end{gathered}$$

where the conditions of (31) and (28) were used. For a non-empty $\mathcal{V}_{k+1}$, (27) implies that $\|\mathbf{v}_{(\mathrm{I})} - \mathbf{p}\| = d_k^2 - \varepsilon^2 \geqslant d_k - \varepsilon \geqslant 0$. Accordingly, the sets of solutions (I)-(III) can be sorted as in

$$\|\mathbf{v}_{(\mathrm{I})} - \mathbf{p}\| = \sqrt{d_k^2 - \varepsilon^2} \geqslant \|\mathbf{v}_{(\mathrm{II})} - \mathbf{p}\| = d_k - \varepsilon > \|\mathbf{v}_{(\mathrm{III})} - \mathbf{p}\| = 0 \tag{34}$$

Therefore, the global solution of (29) is given by

$$\overline{d}_{k+1} = \sqrt{d_k^2 - \varepsilon^2} \tag{35}$$

taking as optimal argument $\mathbf{p}^*_{d,k+1} = \mathbf{v}_{(\mathrm{I})}$ any vector satisfying

$$\begin{cases} (\mathbf{p}^*_{d,k+1} - \mathbf{p}_{d,k})^T\,(\mathbf{p}^*_{d,k+1} - \mathbf{p}_{d,k}) = \varepsilon^2 \\ (\mathbf{p}^*_{d,k+1} - \mathbf{p}_{d,k})^T\,(\mathbf{p} - \mathbf{p}_{d,k}) = \varepsilon^2 \end{cases} \tag{36}$$

The geometrical interpretation of the solution of (29) is illustrated in Figure 9.

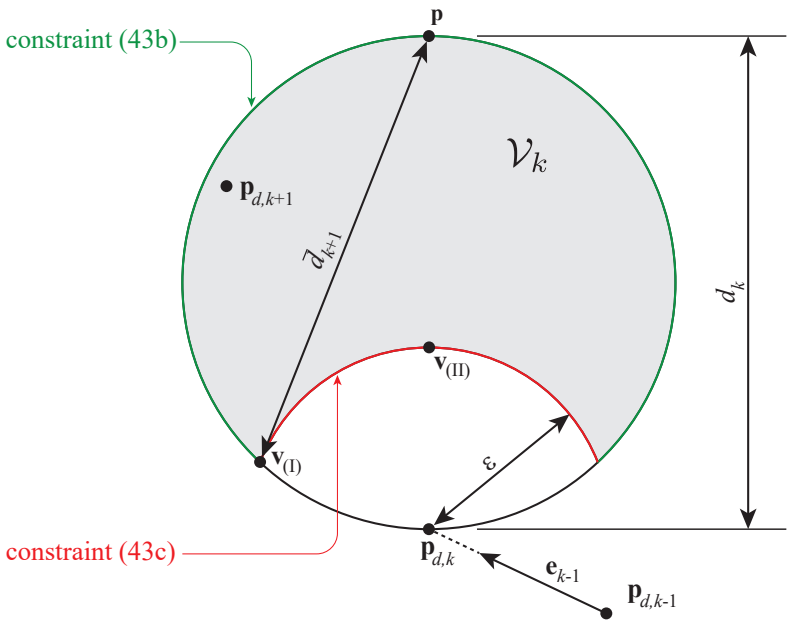

Figure 9: Geometrical interpretation of the solutions of (29).

One may repeat the optimization (29) to obtain $\overline{d}_{k+2}$ substituting $\mathbf{p}^*_{d,k+1}$ into $\mathbf{p}_{d,k}$ for (29b)-(29c), which leads to

$$\overline{d}_{k+2} = \sqrt{\overline{d}^2_{k+1} - \varepsilon^2} \tag{37}$$

Repeating the procedure recursively, one can obtain for any $i > k$

$$\overline{d}^2_{i+1} - \overline{d}^2_i = -\varepsilon^2 \Rightarrow (\overline{d}_{i+1} - \overline{d}_i)(\overline{d}_{i+1} + \overline{d}_i) = -\varepsilon^2 \Rightarrow \tag{38}$$

$$\overline{d}_{i+1} - \overline{d}_i = \frac{-\varepsilon^2}{\overline{d}_{i+1} + \overline{d}_i} \leqslant \frac{-\varepsilon^2}{2\,\overline{d}_k}. \tag{39}$$

Therefore, the sequence $\overline{d}_i$ can be majorized by

$$\overline{d}_i \leqslant d_k - \frac{\varepsilon^2}{2\,d_k}\,(i-k), \tag{40}$$

such that, in accordance with (27)

$$i > \frac{2\,d_k}{\varepsilon^2}(d_k - \varepsilon) + k = \overline{k} \Rightarrow d_i \leqslant \overline{d}_i < \varepsilon \Rightarrow \mathcal{V}_{i+1} = \{\varnothing\}. \tag{41}$$

Therefore, the solution $\hat{k}$ of Algorithm 1 satisfy

$$\hat{k} \leqslant \frac{2\,d_k}{\varepsilon^2}(d_k - \varepsilon) + k, \tag{42}$$

proving the assertion of the theorem. □

B Self-intersecting Curves

The ability to track self-intersecting curves is a crucial characteristic for path following control schemes. Several strategies fail on this matter, *e.g.* [31, 32]. In the case of vector field path following control, for instance, the vector field is singular in crossing points, which leads to a null guidance signal [33].

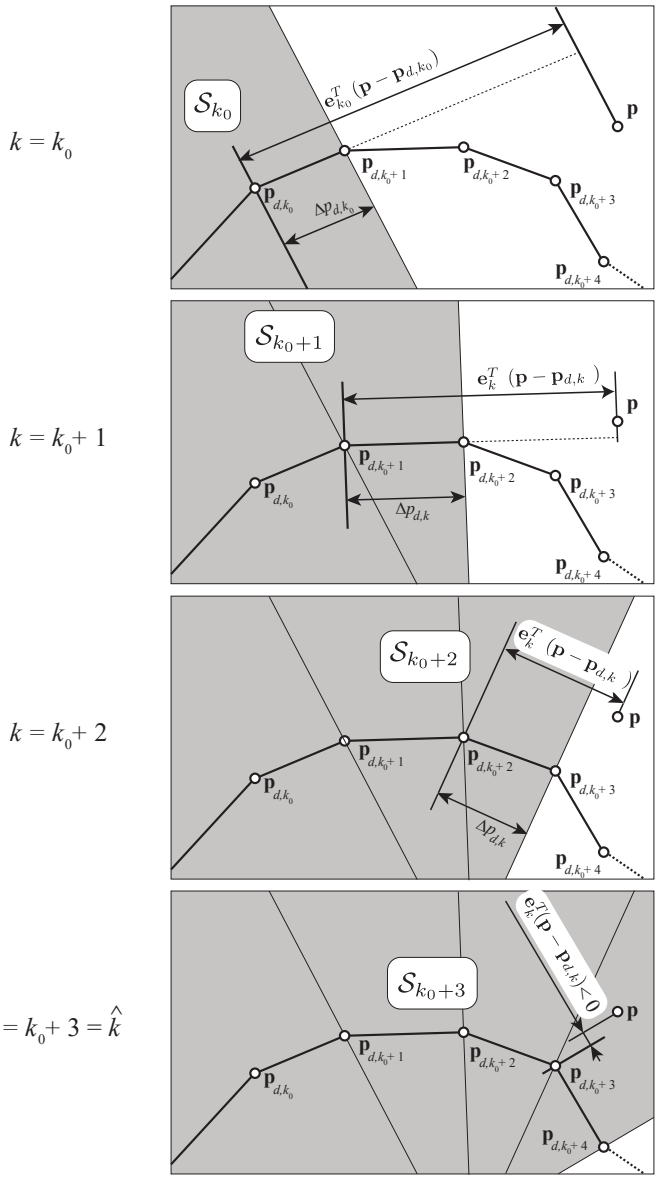

Figure 10: Illustration of a case in which the searched area is extended until $\mathbf{e}_k^T(\mathbf{p} - \mathbf{p}_{d,k}) < \Delta p_{d,k}$ and $\mathbf{p} \in \mathcal{S}_k$ for $\hat{k} = k_0 + 3$.

Similarly to [34], the proposed control scheme is able to track self-intersecting reference curves thanks to the sequential search proposed in Algorithm 1. As a reminder, the applied rationale is illustrated in Figure 10. For $k = \{k_0,\, k_0 + 1, \dots\}$ evaluated sequentially in an increasing order, the algorithm stops whenever $\mathbf{e}_k^T(\mathbf{p} - \mathbf{p}_{d,k}) < \Delta p_{d,k}$.

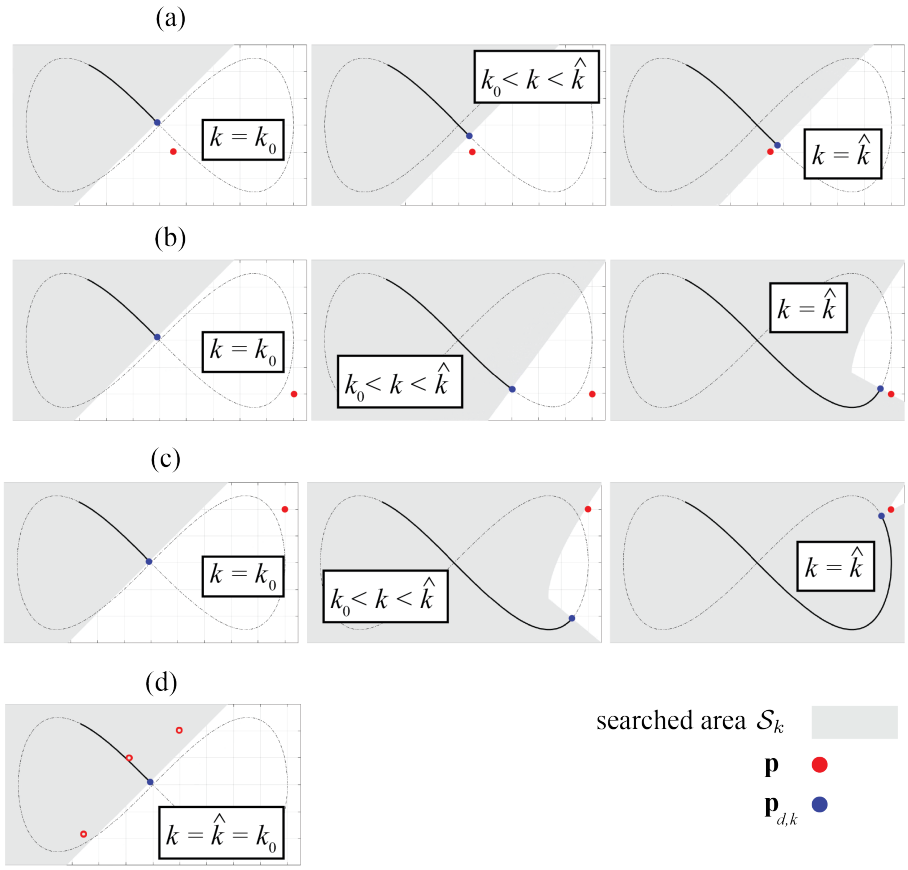

Figure 11: Four different cases indicating that the proposed algorithm is able to track the correct sequence of reference positions for self-intersecting paths. Cases (a), (b) and (c) show that the searched area $\mathcal{S}_k$ is expanded starting from k_0. Case (d) illustrates multiple positions of $\mathbf{p}$ that lead to $\mathbf{e}_{k_0}^T(\mathbf{p} - \mathbf{p}_{d,k_0}) < 0$, such that $\mathbf{p}$ is within the first searched area and Algorithm 1 converges with $k_0 = \hat{k}$.

Consider given step k, $\mathbf{p}_{d,k}$ and $\mathbf{p}_{d,k+1}$. The inequality $\mathbf{e}_k^T(\mathbf{p} - \mathbf{p}_{d,k}) < \Delta p_{d,k}$ determines a region in space delimited by the plane $\mathbf{e}_k^T(\mathbf{p} - \mathbf{p}_{d,k}) = \Delta p_{d,k}$ for which the solution of Algorithm 1 is found. In order to have a record of the accumulated *searched region*, let $\mathcal{S}_k$ be defined by

$$\mathcal{S}_k = \left\{ \mathbf{v} \in \mathbb{R}^3 \,\middle|\, \exists\, j \in \{k_0, k_0 + 1, \ldots, k\} : \mathbf{e}_j^T(\mathbf{v} - \mathbf{p}_{d,j}) < \Delta p_{d,j} \right\} \tag{43}$$

Note that Algorithm 1 converges when reaching a k such that $\mathbf{p} \in \mathcal{S}_k$. Since this condition is tested in an increasing sequence $k = \{k_0, k_0 + 1, \ldots\}$, the algorithm is stopped for the first k satisfying $\mathbf{p} \in \mathcal{S}_k$. Thanks to that, a reference point following the correct sequence in a self-intersecting path is obtained instead of missing a closed portion of the curve. This is shown in Figure 11 and in Video (i)[1].

Taking a k_0 for which $\mathbf{p}_{d,k_0}$ is close to a self-intersecting point, Figure 11 shows how the searched region $\mathcal{S}_k$ is extended until $\mathbf{p} \in \mathcal{S}_k$. Four different cases are considered. In particular, scenario (c) (Case (II) in the video) shows a worst case of the position $\mathbf{p}$ in which $\mathcal{S}_{\hat{k}}$ includes

[1] https://seafile.lirmm.fr/f/a93502cf54ea454abd0b/

Figure 12: Experimental results for a self-intersecting path.

almost the whole plane. Additionally, as shown in case (d), it is worth noting that any $\mathbf{p}$ satisfying $\mathbf{e}_{k_0}^T(\mathbf{p} - \mathbf{p}_{d,k_0}) < 0$ leads to $\hat{k} = k_0$, with Algorithm 1 converging in the first step.

In order to complete the demonstration that the proposed algorithm is able to track a self-intersecting curve, a 3D printing was performed applying the reference path depicted in Figure 12. The printing procedure is available in the Video (ii)[2].

[2]https://seafile.lirmm.fr/f/074035dfe33446c2b2f1/

C External Controllers

An external controller should be integrated to the proposed PPFC in order to control the interaction between the tool and the surface. More precisely, the external controllers proposed as typical applications can be divided with respect to the controlled physical variable as follows:

(i) Distance between the tool position and the surface;

(ii) Applied force perpendicular to the surface.

The next paragraphs discuss more in detail how these types of external controllers can be integrated to the proposed control scheme.

C.1 Distance control

In case (i), the displacements along $\mathbf{n}$ are used to track a distance h_d between the tool and the surface based on the measured distance h_m. Reminding that $\mathbf{n}$ points towards the interior of the object of interest, a simple strategy able to perform the tracking of h_d could apply an external controller position velocity $\dot{\mathbf{p}}_{ec}$ as proposed in the letter:

$$\dot{\mathbf{p}}_{ec} = k_{lh}\,(h_m - h_d)\,\mathbf{n}, \tag{22}$$

with a positive scalar gain k_{lh}. Although (22) applies velocities based uniquely on the measured error $e_h = h_d - h_m$, it is possible to show that $e_h \to 0$ for $t \to \infty$. A draft of the proof of this assertion is presented in the following.

Consider that the errors due to the tracking of the PPFC scheme are negligible. Figure 13 illustrates that the trajectory generated with null velocity along $\mathbf{n}$ leads to a constant distance between the tool and the surface. Since the orientation $\mathbf{n}$ is continuously updated, the translational velocity $\dot{\mathbf{p}}_{PPFC}$ generated by the PPFC controller is kept tangential to the surface. Therefore, the nominal variation of the measured distance is caused uniquely by the external controller velocity $\dot{\mathbf{p}}_{ec}$. More precisely, in accordance with Figure 14,

$$\dot{h}_m = -\|\dot{\mathbf{p}}_{ec}\| = k_{lh}\,(h_d - h_m). \tag{44}$$

For a constant h_d, the closed-loop system (44) leads to

$$\dot{e}_h = \dot{h}_d - \dot{h}_m = -k_{lh}\,(h_d - h_m) = -k_{lh}\,e_h, \tag{45}$$

which is a first order linear system with

$$e_h(t) = e_h(0)\,e^{-k_{hl}t} \Rightarrow \begin{cases} \lim_{t\to\infty} e_h(t) = 0 \\ \lim_{t\to\infty} \dot{\mathbf{p}}_{ec}(t) = \mathbf{0} \end{cases} \tag{46}$$

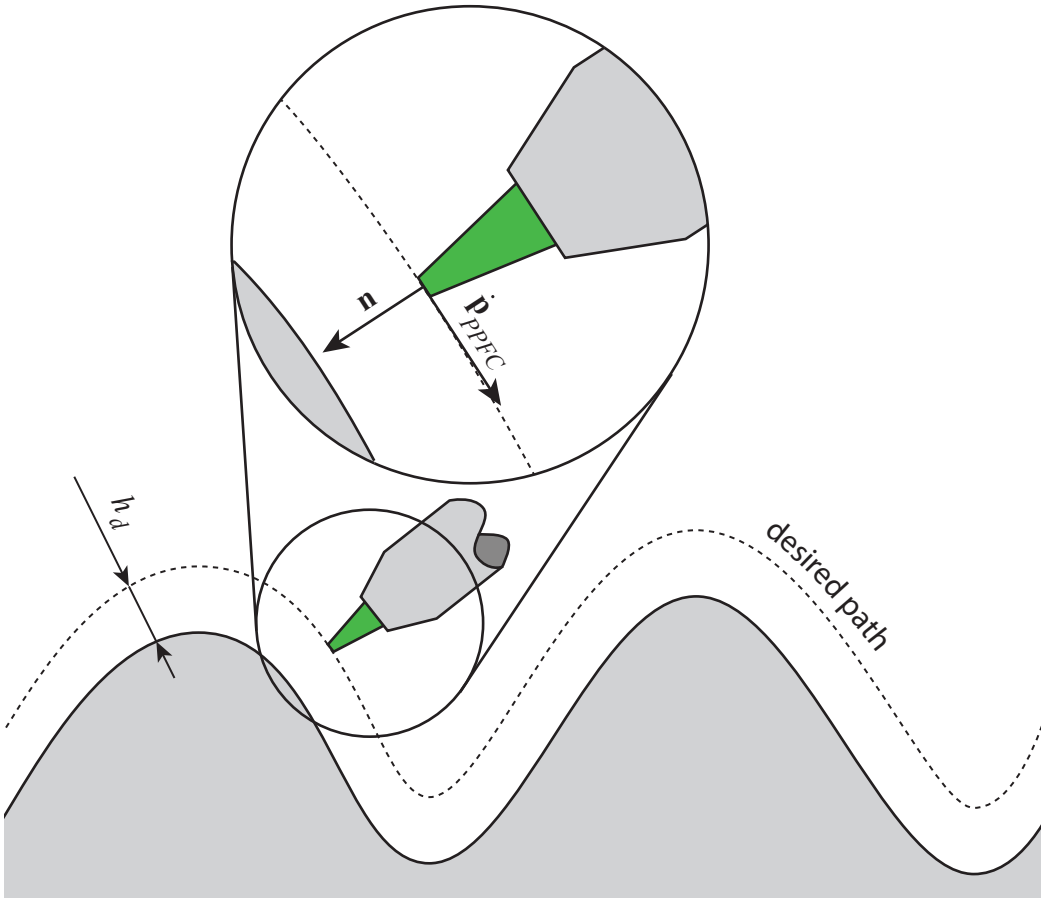

Figure 13: Illustration that if the tracking of $\mathbf{n}$ is able to keep this vector normal to the surface, the PPFC translational velocity is tangential and the h_m is constant.

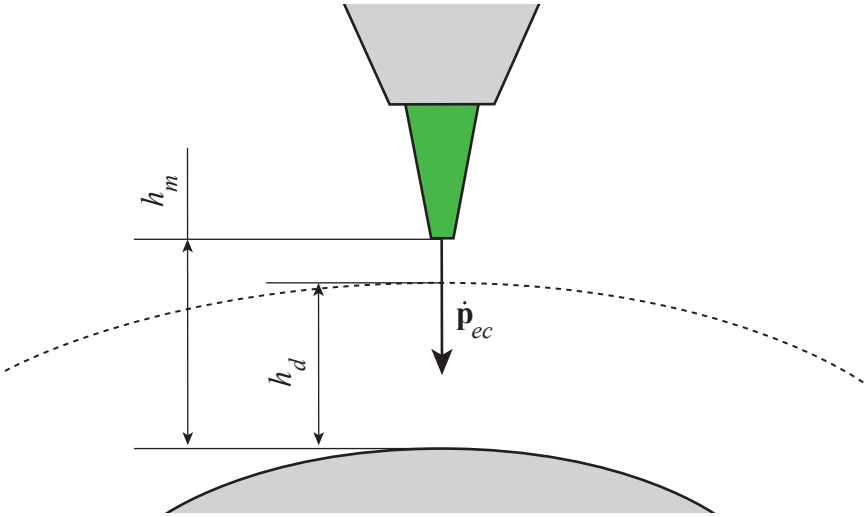

Figure 14: Influence of $\dot{\mathbf{p}}_{ec}$ on the distance h_m.

In short, in spite of the simplicity of (22), this external controller is asymptotically stable if the path following control is able to track the desired positions $\mathbf{p}_{d,k}$ and orientations $\mathbf{n}_{d,k}$ with

sufficient precision.

Clearly, this conclusion depends on the stability of the path following control. The experimental results presented in Section V indicate that the introduced strategy leads to satisfactory results in this matter. A formal stability analysis of the proposed predictive control should be addressed in future works.

C.2 Force control

In case (ii), the displacements along $\mathbf{n}$ are used to control the contact force normal to the surface. A simple strategy able to perform the tracking of a desired force f_d based on a measured force f could apply

$$\dot{\mathbf{p}}_{ec} = k_f(f_d - f)\,\mathbf{n}, \tag{47}$$

with a positive scalar gain k_f. One may apply a rationale similar to the one used in the last section. Nevertheless, the interaction between the tool and the surface leads to additional complexities in this case.

Firstly, one should verify that the precision of the path following control is robust with respect to the friction due to the contact between the tool and the surface. Secondly, the relation between the tool penetration s and the normal force f should be addressed, as illustrated in Figure 15. In order to apply the same rationale used in the last section, one could consider that the normal force can be written as a strictly increasing function of the penetration, *i.e.*

$$f = f(s) : \frac{\mathrm{d}f}{\mathrm{d}s} > 0 \;\forall\; s \geqslant 0. \tag{48}$$

In words, (48) implies that f can be written as function of s such that increased penetrations lead to increased forces. The condition $s \geqslant 0$ is necessary to guarantee that the tool is in contact to the surface.

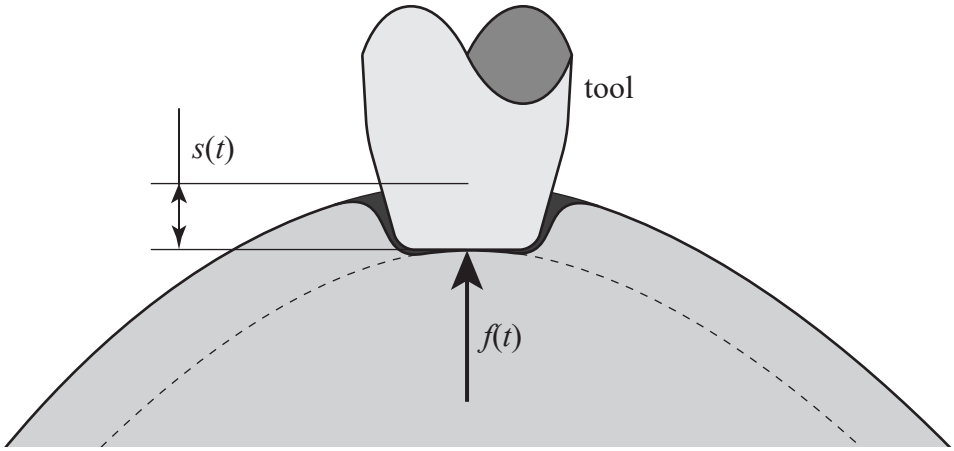

Figure 15: Notations used to correlate the penetration and the normal force.

Additionally, as in relation (44), one can conclude that

$$\dot{s} = \|\dot{\mathbf{p}}_{ec}\| = k_f(f_d - f). \tag{49}$$

Considering the Lyapunov function $V(f) = (f_d - f)^2$ the following conditions can be verified:

$$V(f) = 0 \Leftrightarrow f = f_d \tag{50a}$$
$$V(f) > 0 \Leftrightarrow f \neq f_d \tag{50b}$$

In addition, for $s > 0$, the time derivative of V can be written as

$$\begin{aligned}\dot{V}(f) &= -2\,(f_d - f)\,\dot{f} = -2\,(f_d - f)\,\frac{\mathrm{d}f}{\mathrm{d}s}\,\dot{s} = -2\,(f_d - f)\,\frac{\mathrm{d}f}{\mathrm{d}s}\,k_f(f_d - f)\\ &= -2\,k_f\,\frac{\mathrm{d}f}{\mathrm{d}s}\,(f_d - f)^2,\end{aligned}$$

which, thanks to (48), leads to

$$f = f_d \Leftrightarrow \dot{V}(f) = 0 \tag{51a}$$
$$f \neq f_d \Leftrightarrow \dot{V}(f) < 0. \tag{51b}$$

Relations (50) and (51) prove that the closed-loop system obtained with (47) is asymptotically stable, such that

$$\begin{cases} \lim_{t\to\infty} f(t) = f_d \\ \lim_{t\to\infty} \dot{\mathbf{p}}_{ec}(t) = \mathbf{0} \end{cases} \tag{52}$$

References

[30] J. Nocedal and S. Wright, *Numerical optimization*. Springer Science and Business Media, 2006.

[31] V. M. Goncalves, L. C. A. Pimenta, C. A. Maia, B. C. O. Dutra, and G. A. S. Pereira, "Vector Fields for Robot Navigation Along Time-Varying Curves in n -Dimensions," *IEEE Transactions on Robotics*, vol. 26, no. 4, pp. 647–659, 2010.

[32] W. Yao and M. Cao, "Path following control in 3D using a vector field," *Automatica*, vol. 117, p. 108957, 2020. [Online]. Available: https://www.sciencedirect.com/science/article/pii/S0005109820301552

[33] W. Yao, H. G. de Marina, B. Lin, and M. Cao, "Singularity-Free Guiding Vector Field for Robot Navigation," *IEEE Transactions on Robotics*, vol. 37, no. 4, pp. 1206–1221, 2021.

[34] R. J. Gill, D. Kulić, and C. Nielsen, "Spline path following for redundant mechanical systems," *IEEE Transactions on Robotics*, vol. 31, no. 6, pp. 1378–1392, 2015.